International Journal of Heat and Mass Transfer 146 (2020) 118865

Contents lists available at ScienceDirect

International Journal of Heat and Mass Transfer

journal homepage: www.elsevier.com/locate/ijhmt

Energy flow-based method for analysis and optimization of evaporative cooling and ventilation systems

Fang Yuan *, Wengang Dong, Guangfeng Shen, Yi Li, Wei Liu

School of Energy and Power Engineering, Huazhong University of Science and Technology, Wuhan 430074, China

ARTICLE INFO

Article history:
Received 23 May 2019
Received in revised form 11 September 2019
Accepted 9 October 2019

Keywords:
Evaporation
Energy flow model
Lagrange multipliers method
Thermal resistance
Optimization

ABSTRACT

Physical and mathematical models significantly affect the ease of system analyses and optimization. This contribution presents a modified thermal resistance model for an evaporative cooling process and establishes an energy flow model analogous to an electrical circuit for an indirect evaporative cooling and ventilation (IECV) system based on the overall energy transport. The system modeling equations based on Kirchhoff's laws are a set of linear algebraic equations that characterize the relationships between each component in the system. They are applied as system constraints in the Lagrange multipliers method to optimize the design. The optimization minimizes the total thermal conductance for a fixed cooling capacity and total circulating water mass flow rate. The solutions of the optimization equations for a typical IECV system give a set of Pareto frontiers that reflect the trade-off between the thermal conductance and the mass flow rate, which represent the investment cost and the operating cost. Optimizations with various cooling capacities, indoor temperatures and ambient air conditions reveal their impacts on the optimal parameter allocations. Therefore, this application of the energy flow model shows its advantages for both performance analyses and system optimization.

1. Introduction

Environmental issues have led to the need for renewable energy sources that often require large scale energy storage to replace fossil fuel consumption. Improved standards of living require better thermal comfort capabilities with heating, ventilation and air conditioning systems (HVACs) contributing nearly 50% of the energy consumed in buildings and 10–20% of the total primary energy consumption [1], which implies an enormous potential for energy conservation. HVAC systems using evaporative cooling and ventilation (ECV) are an environmentally-friendly, efficient approach to simultaneously handle heat and moisture loads [2]. Therefore, ECV systems are being rapidly integrated into both residential and commercial buildings in the last few decades.

There have been many studies to evaluate and improve the performance of ECV systems that can be characterized in three aspects. One set is factor studies which explore the influence of ambient air conditions [3], operating parameters such as temperature and water flow rate [4], flow arrangements [5] and packing types and geometries [6] on the cooling performance. The second set involves research on various system layouts, including indirect evaporative cooling [2], dew-point evaporative cooling [7], multi-stage systems [8] and hybrid systems [9,10] that combined evaporative cooling with other HVAC units. The last set is applications of different assessment criteria, for instance, wet-bulb effectiveness [11], dew-point effectiveness [12], exergy efficiency [13] and entransy efficiency [14]. Moreover, to further optimize the system efficiency, some studies have also compared the system performance with various combinations of structural and operating parameters with various objectives such as minimizing the exergy loss [15–17]. However, these trial and error methods cannot easily lead to the optimal theoretical solution.

These analytical and numerical studies all used a modelling method which affects both the performance analysis and the system optimization. In general, HVAC modeling methods [18] can be categorized into data-driven and physics-based approaches. The data-driven approaches use mathematical techniques such as artificial neural networks (ANN) [19], adaptive neuro-fuzzy inference systems (ANFIS) [19] and the group method of data handling-type neural networks (GMDH) [20] to approximately describe the relationship between the input and output variables obtained from a large amount of test data. These methods are accurate within the range of the experimental conditions, but does not reflect either the physical mechanisms relating the components or the system relationships. Physics-based approaches base the

* Corresponding author.
E-mail address: yuanf@hust.edu.cn (F. Yuan).

https://doi.org/10.1016/j.ijheatmasstransfer.2019.118865
0017-9310/

Nomenclature

T	temperature
D	humidity
R	inlet temperature-based thermal conductance
G	heat capacity rate
KA	thermal conductance
Q	heat transfer rate
Greek	
c_p	constant pressure specific heat
γ	evaporation latent heat
m	mass flow rate
h	enthalpy
φ	mass flow rate ratio of ambient air
λ_i	Lagrange multipliers
ε	thermal driving potential
Subscripts	
a	ambient air
w	water
h	hot
c	cold
sat	saturation
wb	wet bulb

modeling equations on the physical laws governing the heat transfer and the heat-work conversion, the fluid dynamics and the component characteristics such as pumps and valves [21–23]. However, this method can lead to unnecessary intermediate variables and over-constrained analytical equations. In addition, the solution process can then require many iterations with long computing times, especially for complex systems. The physics-based approach is component-oriented which models the system by analyzing all the physical processes of each component and then integrating all the governing equations.

Recently, Chen et al. [24] derived a model for the inlet temperature difference-based thermal resistance for a heat exchanger based on the thermal-electrical analogy and developed a power flow method which is successfully applied to the optimizations for heat transfer networks [25], energy storage systems [26], electric-thermal energy systems [27] and ORC systems [28]. The energy flow model is a system-oriented method which can be used to conveniently define the energy network relations using electrical circuit theory while avoid excessive intermediate variables and iterations. However, the energy flow method for thermal systems involving evaporative cooling processes, which involve coupled heat and mass processes, still needs further development. A global optimization method is also needed to obtain the optimal system parameters for various thermal systems [29–32] based on the Lagrange multipliers method. This method requires extra system constraints, i.e., mathematical relations between the structural and operating parameters, which are obtained here from an entransy analysis.

This study first presents a modified thermal resistance model for the coupled heat and mass transfer process and an energy flow model for a typical indirect evaporative cooling and ventilation (IECV) system with several thermal resistances and thermal driving potentials. Then, Kirchhoff's law is used to develop a group of algebraic equations that represents the system relationships for modeling and the optimization constraints. The Lagrange multipliers method is used to optimize the system to obtain the minimum total system thermal conductance for various operating conditions to show the applications and advantages of this modelling method. The impacts of the cooling requirements and the ambient air conditions on the system optimization are also discussed.

2. Energy flow model for an indirect cooling and ventilation system

Fig. 1 is a schematic of a typical indirect evaporative cooling and ventilation system, where A–J, M, N and R represent different

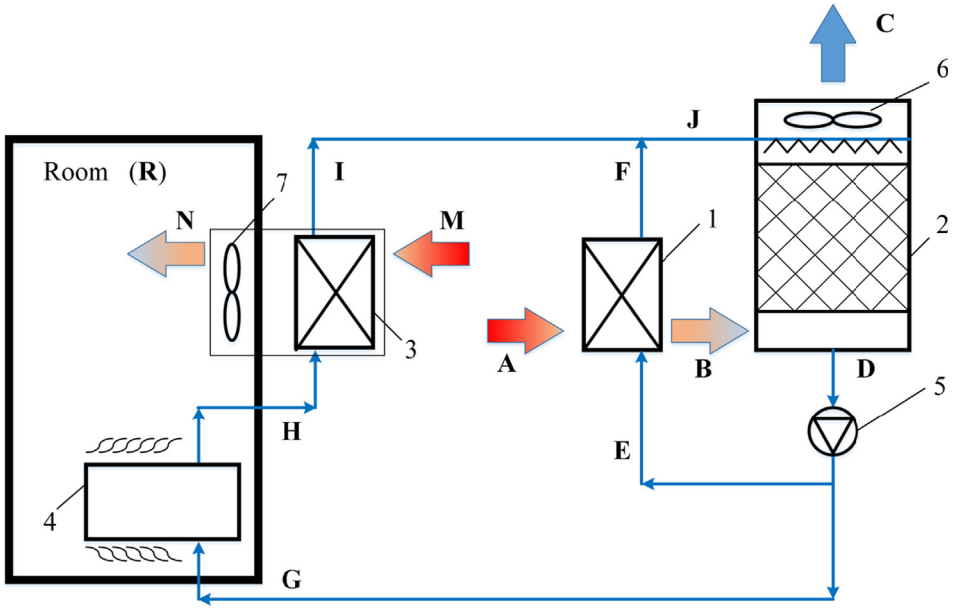

Fig. 1. Schematic of an indirect evaporative cooling and ventilation system. (1-air pre-cooler, 2-direct evaporative cooler, 3-fresh air heat exchanger, 4-fan coil unit, 5-circulating water pump, 6-exhaust fan, 7-fresh air exhaust fan).

states. The system mainly consists of three counter-flow heat exchangers, one coupled heat and mass transfer heat exchanger, two fans and one pump. In this system, ambient air is driven into the direct evaporative cooler (2) by the fan (6) from the air pre-cooler (1). Meanwhile, the circulating water in the direct evaporative cooler (2) will evaporate due to the pressure difference between the water vapor in the ambient air and the saturated water vapor over the circulating water surface. The cooled circulating water is then split into two streams by the circulating water pump (5). One stream is pumped to the air pre-cooler (1) and reduces the air temperature entering the direct evaporative cooler (2) while the other stream flows through the fan coil unit (4) to cool the indoor air and then through the fresh air heat exchanger (3) to cool the fresh air blown into the room. The circulating water flowing out of the fresh air heat exchanger (3) and the air pre-cooler (1) then mix back together and flow back to the direct evaporative cooler (2) to complete the cycle. The whole system produces cooling water to simultaneously remove the room heat load and supply fresh air.

This system energy transport processes include three counter-flow heat transfer processes, one coupled heat and mass transfer process in the direct evaporative cooler and one mixing process of the circulating water. Therefore, different analogous electrical components are introduced to describe the different processes. Some assumptions are made to simplify the analysis: (1) the thermophysical properties of water and air, e.g., the specific heat and the latent heat remain constant; (2) the Lewis number equals one ($Le = 1$) during the coupled heat and mass transfer process; (3) the saturation line of water is linear and follows the relation: $D_{sat} = a \cdot T_{sat} + b$ and (4) the circulating water mass flow rates at states J and D are assumed to be the same, i.e., $m_{w,J} = m_{w,D}$.

2.1. Energy flow analysis of the IECV system

The heat transfer and electrical conduction analogy is used to define the inlet temperature difference-based thermal resistance as [24]:

$$R = \frac{T_{h,i} - T_{c,i}}{Q}, \tag{1}$$

where $T_{h,i}$ and $T_{c,i}$ are the hot and cold fluid inlet temperatures and Q represents the heat transfer rate from the hot fluid to the cold fluid. R then is the heat transfer resistance for this process for the temperature potential difference $T_{h,i} - T_{c,i}$. The energy balance equations for the two fluids can then be used to define R for a counter-flow heat exchanger as

$$R = \frac{G_c e^{\alpha_h} - G_h e^{\alpha_c}}{G_h G_c (e^{\alpha_h} - e^{\alpha_c})}, \tag{2}$$

where G is the heat capacity rate which is the product of the mass flow rate (m) and the specific heat (c_p). Subscripts h and c represent the hot fluid and cold fluids and α is defined as

$$\alpha_i = \frac{KA}{G_i}, \quad i = h, c, \tag{3}$$

where KA denotes the thermal conductance of the heat exchanger which is the product of the heat transfer coefficient (K) and the heat transfer area (A). Unlike the number of transfer units (NTU), α corresponds to the heat capacity rate of each fluid. The thermal resistance only depends on the heat capacity rates of the two fluids and the thermal conductance which represent the operating and structural parameters of the process. For a given heat exchanger, the heat transfer rate can then be directly calculated from the inlet parameters of the two fluids. The air pre-cooler (1), the fresh air heat exchanger (3) and the fan coil unit (4) shown in Fig. 1 are all counter-flow heat exchangers which can be readily characterized by this thermal resistance model.

However, unlike in single-phase heat exchangers, the temperature of the circulating water in the direct evaporative cooler is simultaneously affected by the sensible heat transfer to the ambient air and the latent heat transfer related to the mass transfer of the water vapor. This coupled heat and mass transfer process can be regarded as a single-phase heat transfer process between the water and the ambient air at its wet-bulb temperature with the assumption that Le is equal to one and the saturation line is linear. The equivalent energy balance equation [30] is then

$$Q_2 = m_{a,A} c_{p,ea} \left(T_{a,wb,C} - T_{a,wb,B}\right) = m_{w,J} c_{p,w} \left(T_{w,J} - T_{w,D}\right), \tag{4}$$

where $T_{a,wb}$ is the wet-bulb temperature of the ambient air and T_w is the circulating water temperature. $c_{p,ea} = c_{p,a} + a \cdot \gamma_0$ denotes the equivalent constant pressure specific heat of the ambient air and γ_0 is the latent heat. Subscripts C, B, J and D correspond to the states shown in Fig. 1. The equivalent thermal conductance of this coupled heat and mass transfer process is $c_{p,ea}/c_{p,a}$ times larger than thermal conductance of the direct evaporative cooler, $(KA)_2$. Therefore, the modified thermal resistance model for the direct evaporative cooler is

$$R_2 = \frac{T_{w,J} - T_{a,wb,B}}{Q_2} = \frac{G_{ea} e^{\alpha_w} - G_w e^{\alpha_{ea}}}{G_w G_{ea} (e^{\alpha_w} - e^{\alpha_{ea}})}, \tag{5}$$

where

$$G_{ea} = m_{a,A} c_{p,ea}, \tag{6}$$

$$\alpha_i = \frac{c_{p,ea} (KA)_2}{c_{p,a} G_i}, \quad i = w, ea. \tag{7}$$

The air pre-cooler energy balance can be combined with the isenthalpic humidification process of the ambient air at state B, i.e., $h_{a,B} = h_{a,B,wb}$, to relate the wet bulb temperature of the ambient air at state B, the ambient air inlet parameters and the heat transfer rate in the air pre-cooler (Q_1)

$$T_{a,wb,B} = \frac{m_{a,A} \left[c_{p,a} T_{a,A} + \gamma_0 D_{a,A} + (273.15a - b)\gamma_0\right] - Q_1}{m_{a,A} c_{p,ea}}, \tag{8}$$

where D_a represents the ambient air humidity. Then, the heat transfer and the coupled heat and mass transfer process between the two fluids can be described using the thermal resistance model to relate the various nodal potentials for the inlet temperatures of the two fluids.

The energy equations for the water stream in the heat exchangers are then used to define the circulating water temperature differences resulting from the heat transfer

$$\varepsilon_1 = T_{w,F} - T_{w,E} = \frac{Q_1}{m_{w,E} c_{p,w}}, \tag{9}$$

$$\varepsilon_3 = T_{w,I} - T_{w,H} = \frac{Q_3}{m_{w,H} c_{p,w}}, \tag{10}$$

$$\varepsilon_4 = T_{w,H} - T_{w,G} = \frac{Q_4}{m_{w,G} c_{p,w}}, \tag{11}$$

where ε are the thermal driving potentials that characterize the temperature increases in the energy network like voltage sources in an electrical circuit which are determined by the corresponding heat transfer rates and mass flow rates in each heat exchanger. Similarly, the temperature changes due to the mixing of the circulating water streams at states F and I can be described by two thermal driving potentials as

$$\varepsilon_{mix1} = T_{w,J} - T_{w,F} = \frac{Q_2}{m_{w,D} c_{p,w}} - \frac{Q_1}{m_{w,E} c_{p,w}}, \tag{12}$$

and

$$\varepsilon_{mix2} = T_{w,J} - T_{w,I} = \frac{Q_2}{m_{w,D}c_{p,w}} - \frac{Q_3 + Q_4}{m_{w,G}c_{p,w}}, \tag{13}$$

where Q_3 and Q_4 are the heat transfer rates in the fresh air heat exchanger and the fan coil unit. The energy flow model for the IECV system can then be given by connecting the state nodes at the same temperatures as shown in Fig. 2.

In the figure, the red lines stand for the heat sources (indoor air and ambient air) while the black lines indicate the circulating water. ε_1, ε_3 and ε_4 represent the temperature changes of the circulating water passing through the air pre-cooler, the fresh air heat exchanger and the fan coil unit. R_1–R_3 are the thermal resistances for each heat transfer process, while R_4 is the thermal resistance of the coupled heat and mass transfer process. This model intuitively shows both the energy transport directions and the connecting relations between each component. In addition, the lower temperature limit of the cooling water from this IECV system is the wet bulb temperature of state B. Furthermore, since this model is similar to an electrical network, Kirchhoff's laws for electrical circuit theory can be used to derive the system equations for modeling the IECV system.

2.2. Modeling of the IECV system

Kirchhoff's current law relates the flow rates in each branch of the energy network as,

$$Q_1 + Q_3 + Q_4 - Q_2 = 0, \tag{14}$$

This is the same as the overall system energy conservation equation. Kirchhoff's voltage law relates the nodal temperature as

$$T_{a,R} - Q_4R_4 + \varepsilon_1 + \varepsilon_{mix1} - Q_2R_2 = T_{a,wb,B}, \tag{15}$$

$$T_{a,A} - Q_1R_1 + \varepsilon_1 + \varepsilon_{mix1} - Q_2R_2 = T_{a,wb,B}, \tag{16}$$

$$T_{a,M} - Q_3R_3 + \varepsilon_3 + \varepsilon_{mix2} - Q_2R_2 = T_{a,wb,B}, \tag{17}$$

where thermal resistances R_1, R_3 and R_4 are obtained by substituting the corresponding heat capacity rates and thermal conductances into Eq. (2). For a given IECV system with given ambient air conditions and mass flow rates of the circulating water in the two streams, Eqs. (14)–(17) can be combined with Eq. (8) to calculate the heat transfer rate in each heat exchanger.

The energy flow model relates the inlet parameters, the structural parameters, i.e., the thermal conductance and the operating parameters, i.e., the mass flow rates of the two circulating water streams to the system output, i.e., the cooling capacity, through a set of linear algebraic equations. Unlike conventional physical-based methods, this method establishes the governing energy transport equations from a system-level perspective. This model then reflects both the characteristics of the various processes and the relationships between each component with the minimum number of unknowns, while conventional models include the immediate temperatures of the circulating water at all the various states in the cycle since physical models of the whole system model the components one by one. Therefore, the energy flow model effectively simplifies the calculation, especially for hybrid thermal systems involving IECV and multi-stage ECV systems.

2.3. Model verification

The energy flow model for a plate-fin heat exchanger has already been validated experimentally [33]. The reliability of the IECV energy flow model is verified here by comparing with previous numerical results [34] in Fig. 3 and experimental data [16] in Table 2. The ambient air and circulating water inlet parameters are listed in Table 1. The results indicate that the energy flow model predictions agree well with both the earlier predictions and the experimental data with relative errors of less than 5% for the other model and 7.4% for the experimental data.

3. Optimization model for the IECV system

IECV system designs should consider both the investment cost and the operating cost. The investment cost mainly depends on the heat exchanger heat transfer areas while the operating cost mainly depends on the energy consumed by the circulating water pump. However, these two conflicting optimization objectives cannot normally be simultaneously optimized for a given system cooling load.

Therefore, in this study, the system is optimized for a given total circulating water flow rate with the aim to minimize the total thermal conductance of all the heat exchangers. This is a typical constrained optimization problem which can be solved using the Lagrange multipliers method from optimization theory.

For an IECV system with a fixed cooling capacity,

$$Q_3 + Q_4 = Q_c = \text{const}, \tag{18}$$

and a given total mass flow rate of circulating water,

$$m_{w,E} + m_{w,G} = m_{w,J} = \text{const}, \tag{19}$$

the mass flow rate ratio of the ambient air blown into the air pre-cooler to the total mass flow rate of ambient air is

$$\varphi = \frac{m_{a,A}}{m_a}. \tag{20}$$

Then, a Lagrange function with the objective of minimizing the total thermal conductance can be constructed using Eqs. (15)~(17) as the system constraints

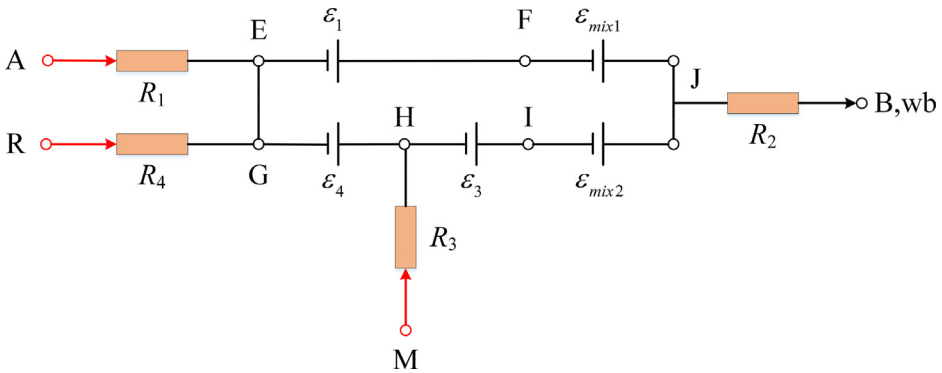

Fig. 2. IECV energy flow model.

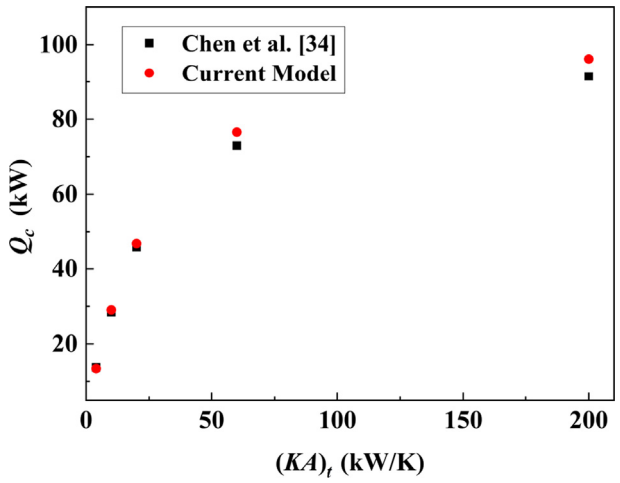

Fig. 3. Comparison of the predicted cooling capacity with previous numerical results [34].

$$F = \begin{bmatrix} \sum_{i=1}^{4} (KA)_i + \lambda_1 \left(m_{w,E} + m_{w,G} - m_{w,J} \right) \\ +\lambda_2 \left(t_{a,R} - Q_4 R_4 + \varepsilon_1 + \varepsilon_{mix1} - Q_2 R_2 - t_{a,wb,B} \right) \\ +\lambda_3 \left(t_{a,A} - Q_1 R_1 + \varepsilon_1 + \varepsilon_{mix1} - Q_2 R_2 - t_{a,wb,B} \right) \\ +\lambda_4 \left(t_{a,M} - Q_3 R_3 + \varepsilon_3 + \varepsilon_{mix2} - Q_2 R_2 - t_{a,wb,B} \right) \end{bmatrix}, \quad (21)$$

where, λ_1–λ_4 are the Lagrange multipliers. The energy flow model gives all the necessary equations with no need to derive extra mathematical relations for the system relationships.

Setting the differentials of Eq. (21) with respect to the thermal conductances of each heat exchanger, the mass flow rates in the two streams, the air flow rate ratio, φ, and the heat transfer rates Q_1 and Q_3 to zero yields

$$\begin{cases} \frac{\partial F}{\partial (KA)_i} = 0, & i = 1,2,3,4 \\ \frac{\partial F}{\partial m_{w,j}} = 0, & j = E,G \\ \frac{\partial F}{\partial \varphi} = 0 \\ \frac{\partial F}{\partial Q_k} = 0, & k = 1,3 \end{cases}, \quad (22)$$

where the specific expressions in Eq. (22) are shown in the Appendix A as Eqs. (A.1)–(A.9).

Simultaneously solving the thirteen optimization equations, Eqs. (15)–(17), (19) and (22), gives the optimal design conditions for the minimum total thermal conductance and the corresponding optimal allocation for each heat exchanger, the mass flow rates of circulating water in the two streams and the ambient air mass flow rate.

Fig. 4 shows the flow chart for both the modeling and optimization processes for the IECV system. When the ambient air conditions and the cooling requirements including the temperature and cooling capacity are prescribed, the equations can be easily solved for both performance analyses and preliminary designs without any iterations.

4. Optimization results and discussion

The model was solved for an inlet temperature for the indirect evaporative cooling and ventilation system shown in Fig. 1 of 308 K, an inlet humidity of 0.007 kg/kg and a total air mass flow rate of 7 kg/s. The required cooling capacity was 93.4 kW and the indoor temperature was 297 K. The heat capacity rate of the room air was assumed to be infinite. Fig. 5 shows the variation of the minimum total thermal conductance for various water mass flow rates. As the water mass flow rate, m_w, increases, the total thermal conductance, $(KA)_t$, first decreases sharply and then slowly increases. Thus, there is an optimal mass flow rate, $m_{w,P1}$, which minimizes the required $(KA)_t$, which is referred to as point P_1. The corresponding operating and structural parameters for this point are listed in Table 3.

When the given $(KA)_t$ is lower than total thermal conductance at point P_1, $(KA)_{t,P1}$, the system cannot satisfy the cooling requirement for any water mass flow rate. When the given $(KA)_t$ is higher than $(KA)_{t,P1}$, there are two different m_w on the optimal curve corresponding to the same $(KA)_t$. The smaller water mass flow rate will have a lower circulating water pump energy consumption and, consequently, will be more efficient. Therefore, the optimal conditions to the left of point P_1 are consistent with the optimization principle that an increasing mass flow rate reduces the required $(KA)_t$. When the given m_w is larger than $m_{w,P1}$, a higher mass flow rate requires a larger thermal conductance to satisfy the cooling capacity, which means that increasing m_w has a negative effect on the optimization of $(KA)_t$. Thus, the left optimal curve is essentially the Pareto frontier which reflects the trade-off between the thermal conductance and the mass flow rate, which represent the investment cost and the operating cost. In these calculations, the total air mass flow rate was prescribed, so the variations of the total energy consumed by the two fans with different flow rates was not considered. In addition, a lower m_w results in a steeper increase of $(KA)_t$ along with a minimum m_w for a fixed cooling requirement, such as point P_2 in Fig. 5. Thus, the system can be operated in the three regions shown in Fig. 5. The system in Region I will not meet the design requirement unless the designer increases $(KA)_t$ and/or m_w. The system in Region II can be optimized by minimizing $(KA)_t$ and/or m_w. The system in Region III should be avoided because m_w in this region exceeds the optimal mass flow rate, $m_{w,P1}$.

When the air inlet parameters, the required indoor temperature, the flow rate allocation ratios of ambient air and circulating water and Q_2 are fixed at the values for point P_1 in Fig. 5, the system still has eight variables that need to be determined, $m_{w,D}$, $(KA)_1$, $(KA)_2$, $(KA)_3$, $(KA)_4$, Q_1, Q_3, and Q_4 with five constraint equations, Eqs. (8), (14)–(17); thus, the system still has three independent parameters. Table 4 lists nine arbitrary combinations of $m_{w,D}$, $(KA)_1$ and $(KA)_3$ that differ from those of point P_1 with Fig. 6 showing the total thermal conductances of the two other heat exchangers in each case, where the horizontal dashed line represents the total thermal conductance for point P_1, $(KA)_{t,P1}$. The total thermal conductance optimized by the energy flow model-based Lagrange multipliers method is indeed the minimum.

Table 1
Model inlet parameters for comparison to the present model.

Model	Ambient air				Circulating water	User inputs	
	Inlet air flow rate (kg/s)	Fresh air flow rate (kg/s)	Humidity (kg/kg)	Temperature (°C)	Mass flow rate (kg/s)	Mass flow rate at point R (kg/s)	Temperature at point R (°C)
Numerical model [34]	1.9	0	0.008	32	2	1.55	32
Experimental data [16]	14.5	6.64	0.010	32.35	5.56	∞	23

Table 2
Predicted and measured temperatures for an IVEC system.

	$t_{w,D}$ (°C)	$t_{w,F}$ (°C)	$t_{w,H}$ (°C)	$t_{w,J}$ (°C)	$t_{a,B}$ (°C)
Experimental data [16]	17.30	28.17	22.63	25.55	19.25
Current model	17.38	27.92	20.97	25.35	19.27
Relative error	0.44%	−0.89%	−7.33%	−0.78%	0.10%

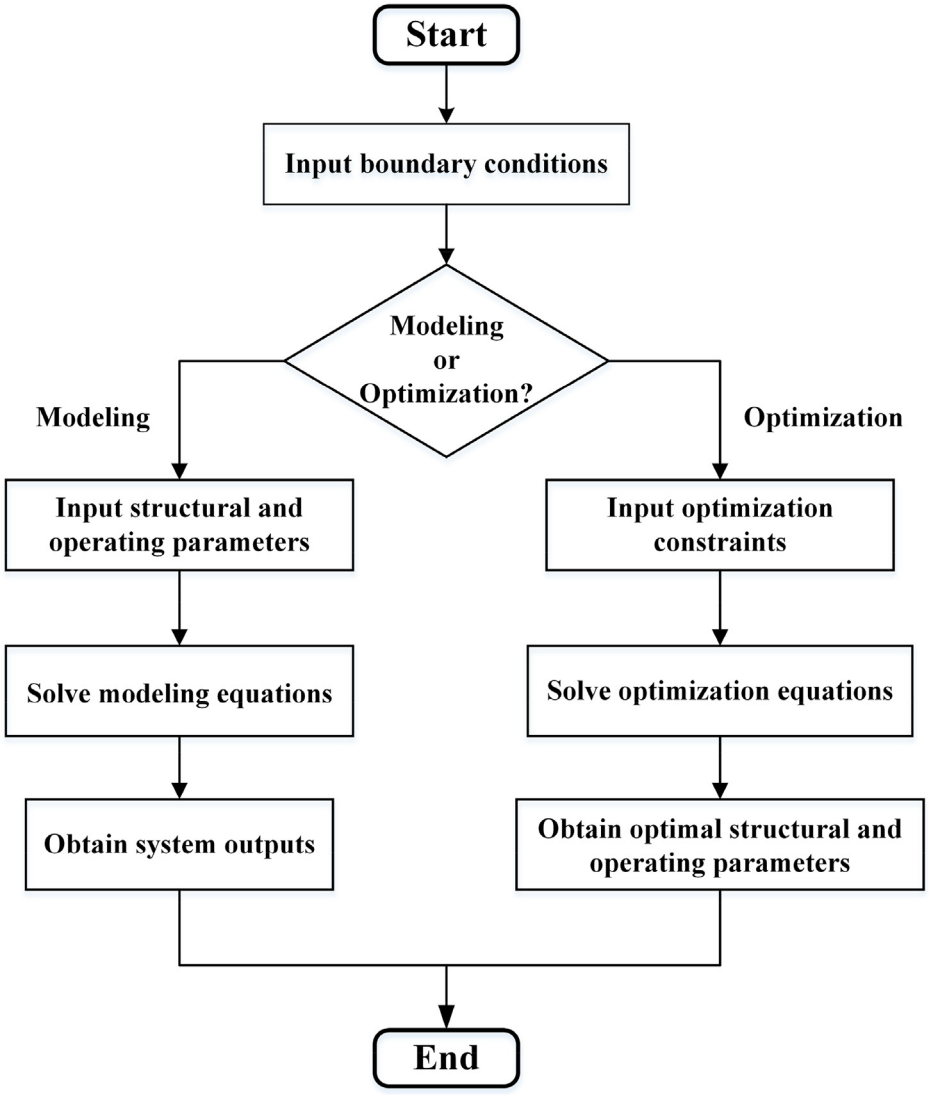

Fig. 4. Solution method flow chart for modeling and optimization.

Since the curve to the right of point P_1 is not useful for system optimization, only the left part of the optimal curve will be analyzed. Fig. 7 shows the optimal thermal conductance allocation for each heat exchanger for different water mass flow rates. Increasing m_w leads to lower thermal conductances of the air pre-cooler, the direct evaporative cooler and the fresh air heat exchanger and a higher thermal conductance of the fan coil unit. Figs. 8 and 9 show the optimal mass flow rate allocations of the circulating water and the ambient air for various water mass flow rates. Increasing m_w leads to higher water mass flow rates in both branches with the mass flow rate ratio of the circulating water flow to the air pre-cooler to the total mass flow rate varying only slightly over a small range. In addition, a larger air mass flow rate due to the increasing m_w is needed to cool the circulating water so as to improve the system refrigeration capacity as shown in Fig. 9.

Fig. 10 shows the influence of the indoor temperature on the system optimization. Reducing the indoor temperature results in a decrease of the minimum total thermal conductance and an increase of the water mass flow rate. A lower indoor temperature requires a lower water temperature from the evaporative cooler; therefore, its heat transfer area needs to be significantly larger. Increasing the heat transfer area with a fixed cooling capacity leads to a lower water mass flow rate. Thus, a higher indoor temperature allows the system to be operated with a wider range of water mass flow rates. Fig. 11 shows the fresh air temperature entering the room, $T_{a,N}$, versus the water mass flow rate for various indoor temperatures. $T_{a,N}$ is always equal to the indoor air temperature, which indicates that the optimization analysis should eliminate the irreversibility of the mixing of the fresh air and the indoor air; although, the non-isothermal mixing of the circulating water from

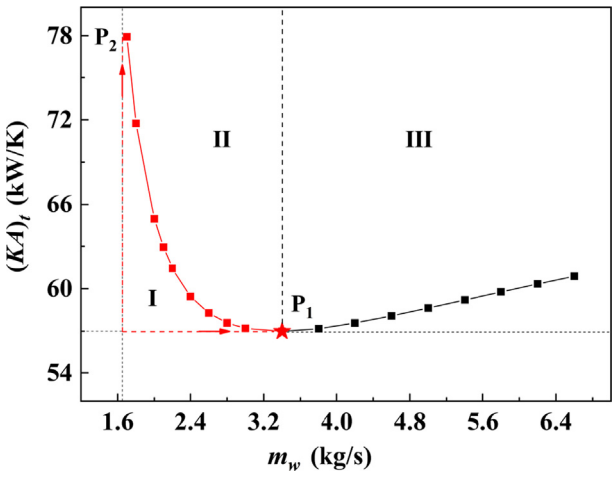

Fig. 5. Minimum total thermal conductance for various water mass flow rates.

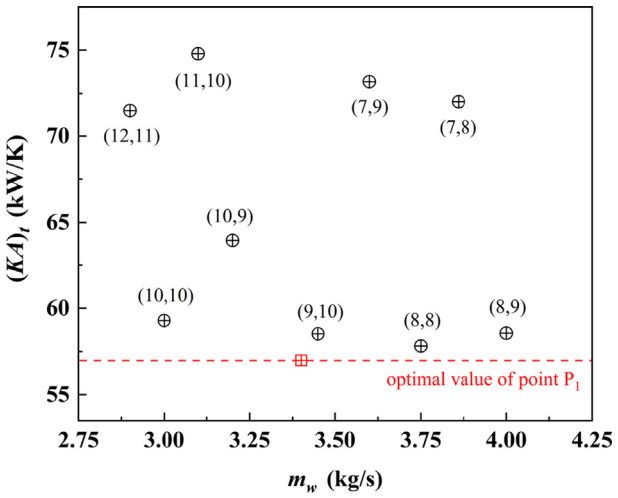

Fig. 6. Comparisons of the total thermal conductance of the nine random cases listed in Table 4 with the optimal value for point P_1.

the two branches is still necessary. Therefore, the system should be optimized as a whole rather than by individual components as is often done in the literature.

Fig. 12 shows the influence of the required cooling capacity on the system optimization. Both the minimum total thermal conductance and its corresponding circulating water mass flow rate increase as the required cooling capacity increases. When the required indoor temperature is fixed, increasing the required cooling capacity will increase the heat transfer temperature difference in the fresh air heat exchanger and the fan coil unit and, consequently, reduce the required cooling water temperature produced by the system. Thus, the system needs more circulating water and more heat transfer area to increase the refrigeration capacity.

Figs. 13 and 14 show the optimal thermal conductance allocation ratios for each heat exchanger and the optimal mass flow rate allocation ratios of the circulating water and the ambient air for various cooling capacities. Increasing the required cooling capacity linearly reduces the optimal thermal conductance allocation ratio of the fresh air heat exchanger while linearly increasing that of the fan coil unit. The optimal thermal conductance allocation ratios of the air pre-cooler and the direct evaporative cooler remain almost constant. Therefore, different cooling requirements can be achieved mainly by adjusting the heat exchanger heat transfer areas. Increasing the required cooling capacity leads to a large increase in the optimal ambient air flow rate allocation ratio while the optimal water flow rate allocation ratio remains almost constant, as shown in Fig. 14.

The impacts of the ambient air conditions on the system optimization were also analyzed with all the other conditions the same as in Fig. 5. Figs. 15 and 16 show the variation of the minimum total thermal conductance and its corresponding circulating water mass flow rate for various ambient air temperatures and

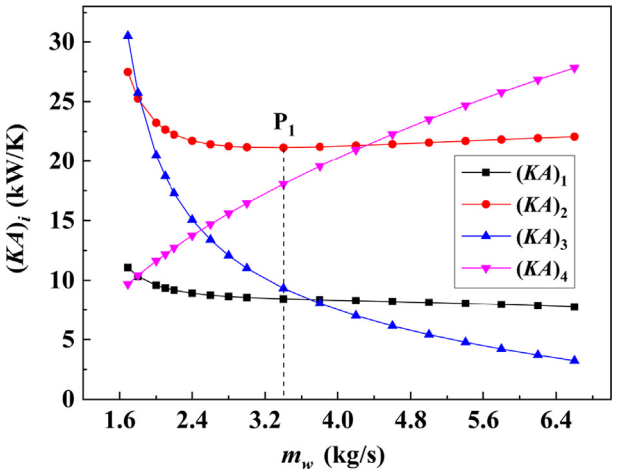

Fig. 7. Optimal thermal conductances of each heat exchanger for various water mass flow rates.

humidities. As the ambient air temperature rises, the minimum thermal conductance first increases and then rapidly decreases while the corresponding water mass flow rate continuously decreases. The reason is that as the ambient air temperature rises, more cooling capacity is required to cool the air blown into the room and the fresh air heat exchanger needs more heat transfer area. Then, the fan coil unit cooling capacity will be lower since the total cooling capacity is fixed so the fan coil unit thermal

Table 3
Optimal IECV system conditions.

Design parameters	$(KA)_t$ (kW/K)	$(KA)_1$ (kW/K)	$(KA)_2$ (kW/K)	$(KA)_3$ (kW/K)	$(KA)_4$ (kW/K)	$m_{w,E}$ (kg/s)	$m_{w,G}$ (kg/s)	$m_{a,A}$ (kg/s)	$m_{a,M}$ (kg/s)
Optimum	56.98	8.45	21.15	9.47	17.91	0.75	2.61	3.71	3.29

Table 4
Nine different combinations of $m_{w,D}$, $(KA)_1$ and $(KA)_3$.

Case No.	1	2	3	4	5	6	7	8	9
$m_{w,D}$ (kg/s)	2.9	3	3.1	3.2	3.45	3.6	3.75	3.86	4
$(KA)_1$ (kW/K)	12	10	11	10	9	7	8	7	8
$(KA)_3$ (kW/K)	11	10	10	9	10	9	8	8	9

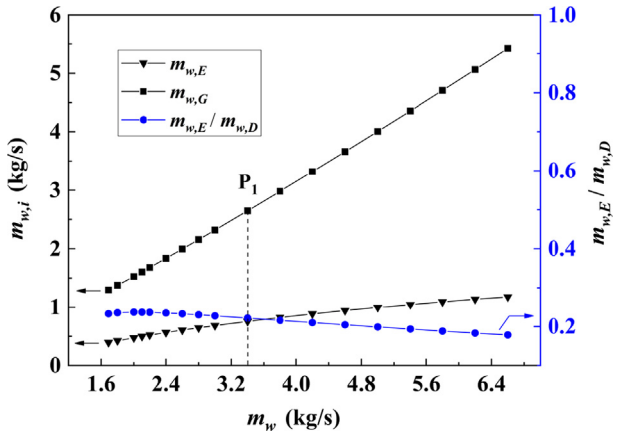

Fig. 8. Optimal mass flow rate allocation of the water flow rate to the air pre-cooler for various total water mass flow rates.

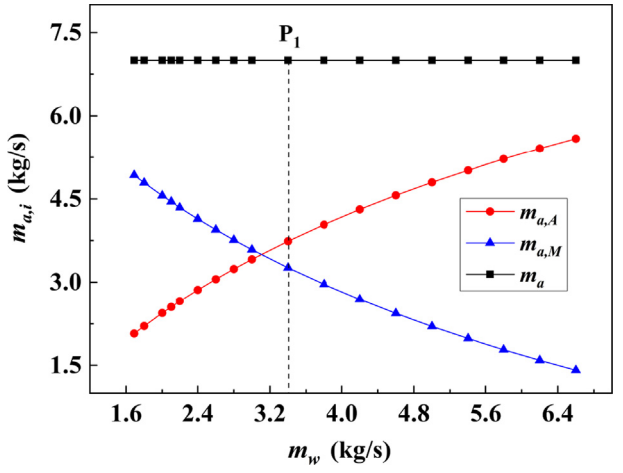

Fig. 9. Optimal mass flow rate allocation of the air for various water mass flow rates.

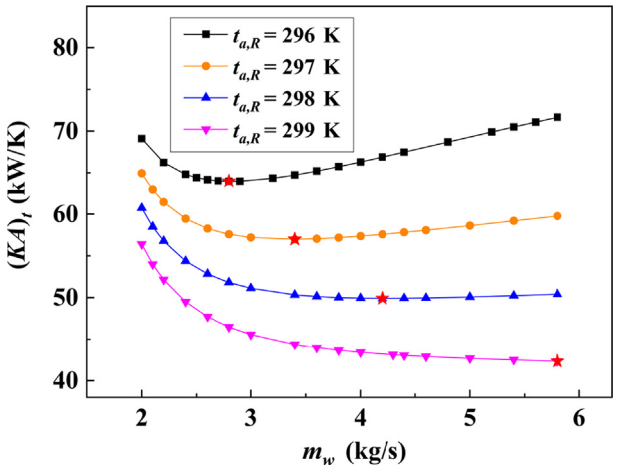

Fig. 10. Minimum total thermal conductance for various water mass flow rates and indoor air temperatures.

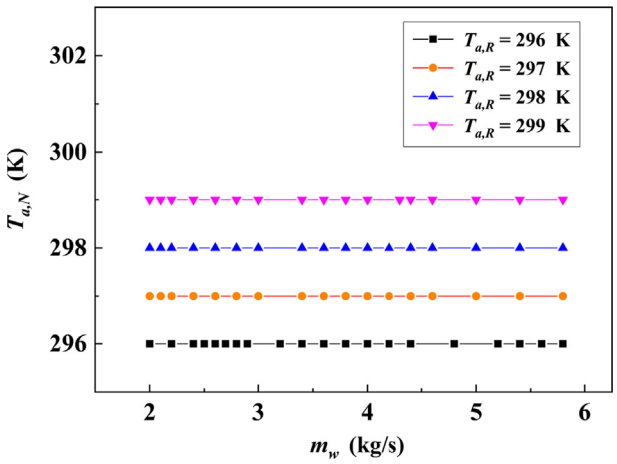

Fig. 11. Fresh air temperature entering the room for various water mass flow rates and indoor air temperatures.

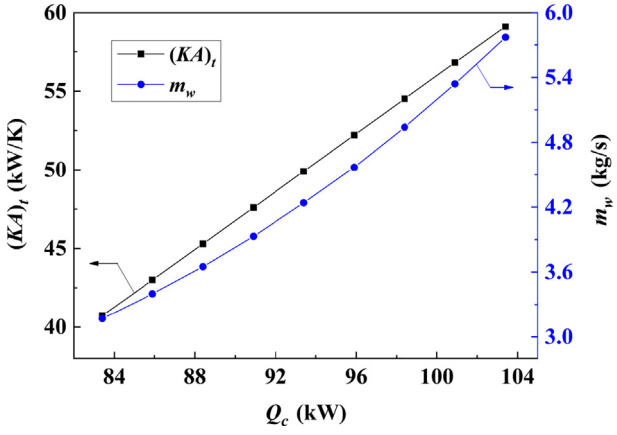

Fig. 12. Minimum total thermal conductance and its corresponding circulating water mass flow rate for various required cooling capacities.

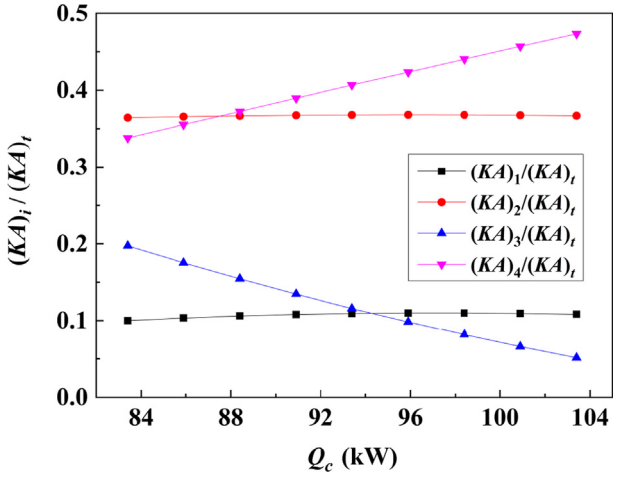

Fig. 13. Optimal thermal conductance allocation ratios for each heat exchanger to its corresponding minimum total thermal conductance for various cooling capacities.

conductance will also be lower. The fresh air heat exchanger cooling capacity is a large part of the total required cooling capacity; therefore, the water mass flow rate is reduced. Furthermore, higher humidity ambient air needs a larger total thermal conductance but almost no impact on the optimal water mass flow rate as shown in Fig. 16. This is because increasing the ambient air humidity reduces the mass transfer potential in the direct evaporative cooler

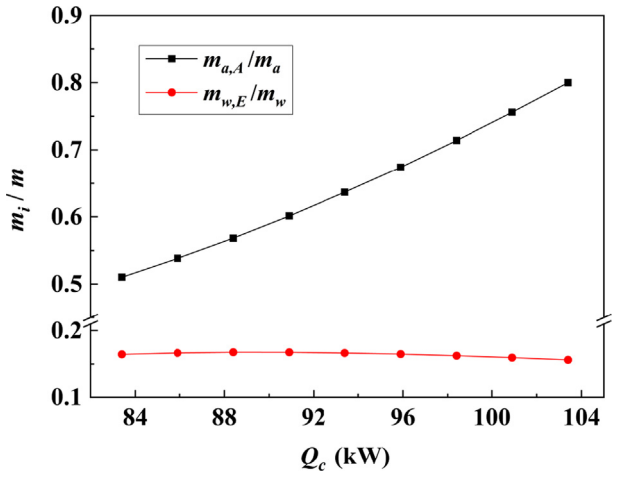

Fig. 14. Optimal mass flow rate allocation ratios of the circulating water and the ambient air for various cooling capacities.

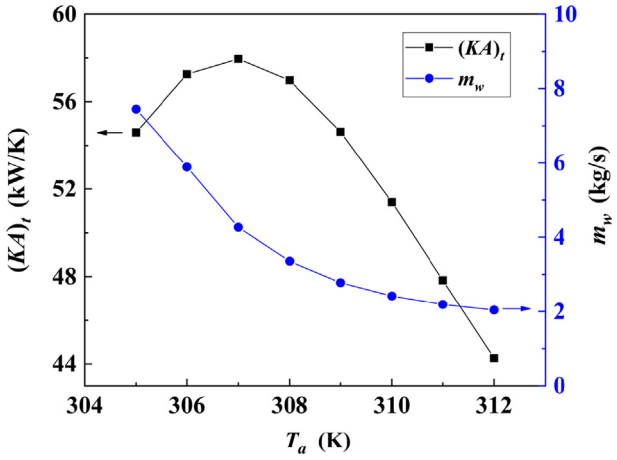

Fig. 15. Minimum total thermal conductance and its corresponding circulating water mass flow rate for various ambient air temperatures.

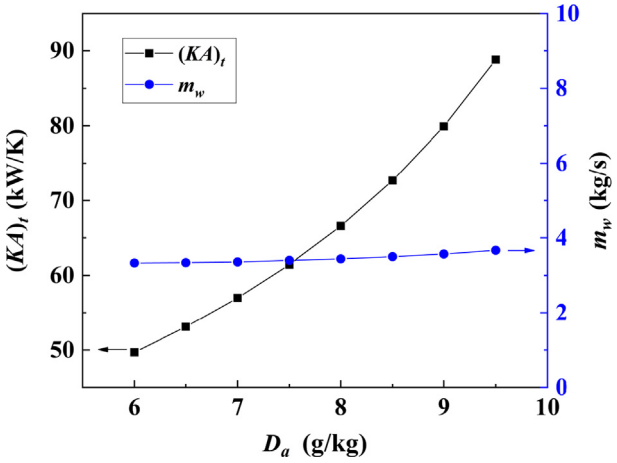

Fig. 16. Minimum total thermal conductance and its corresponding circulating water mass flow rate for various ambient air humidities.

which reduces the heat transfer due to the latent heat. Therefore, the total thermal conductance has to be increased to obtain the same cooling capacity.

This analysis shows that the optimal allocations of the thermal conductance and the mass flow rate in the system are both influenced by not only the cooling capacity and temperature requirements but also by the system boundary conditions given by the ambient air conditions. The energy flow model optimization can conveniently take all these factors into consideration simultaneously.

5. Conclusions

The thermal-electrical analogy for heat transfer was used to develop a thermal resistance model for direct evaporative cooling processes by taking the temperature difference between the circulating water temperature and the ambient air wet-bulb temperature as the driving potential for the coupled heat and mass transfer processes. Then, an energy flow model was developed to analyze the system performance and optimize the system design using several thermal resistances and thermal driving potentials. This model not only identifies the governing heat transport law for the entire system, but also shows the constitutive relations for each process in the system that are not given in conventional physical-based models.

Kirchhoff's laws for electrical circuit theory were then used to develop a set of linear algebraic equations that reflect both the system structure and the characteristics of each component in the IECV system. These were then used as the system constraints for the Lagrange multiplier method to develop an optimization equation set to minimize the total thermal conductance for a fixed circulating water mass flow rate.

Simultaneous solutions of the optimization equations give the Pareto frontier that represents the trade-off between the minimum total thermal conductance and the minimum total circulating water mass flow rate for a required cooling capacity of the IECV system, as well as the corresponding water mass flow rate allocation and the thermal conductance allocation for each heat exchanger. In addition, optimizations with various ambient air conditions and cooling requirements show that a higher ambient air temperature reduces both the required total thermal conductance of the heat exchangers and the circulating water flow rate when $T_{a,A}$ is higher than 307 K, while higher humidity air needs higher thermal conductances. In addition, a higher required indoor air temperature leads to a lower thermal conductance and a larger circulating water flow rate; while increasing the required cooling capacity increases both the thermal conductance and the circulating water flow rate.

Declaration of Competing Interest

The authors declared that there is no conflict of interest.

Acknowledgments

The present work was supported by the National Natural Science Foundation of China (Grant Nos. 51506061 & 51736004).

Appendix A

The differential of Eq. (22) with respect to the thermal conductance $(KA)_1$ yields

$$\frac{\partial F}{\partial (KA)_1} = 1 - \lambda_3 Q_1 \left[\frac{\left(G_{w,E}^2 e^{\alpha_{a,A}} - G_{a,A}^2 e^{\alpha_{w,E}}\right)\left(e^{\alpha_{a,A}} - e^{\alpha_{w,E}}\right) - \left(G_{w,E} e^{\alpha_{a,A}} - G_{a,A} e^{\alpha_{w,E}}\right)^2}{G_{w,E}^2 G_{a,A}^2 \left(e^{\alpha_{a,A}} - e^{\alpha_{w,E}}\right)^2} \right], \tag{A.1}$$

where

$$G_{a,A}=\varphi m_a c_{p,a},\ G_{w,E}=m_{w,E}c_{p,w},\ \alpha_{a,A}=\frac{(KA)_1}{\varphi m_a c_{p,a}},\ \alpha_{w,E}=\frac{(KA)_1}{m_{w,E}c_{p,w}}.$$

The differential of Eq. (22) with respect to the thermal conductance $(KA)_2$ yields

$$\frac{\partial F}{\partial (KA)_2}=1-\frac{c_{p,ea}}{c_{p,a}}(Q_1+Q_c)(\lambda_2+\lambda_3+\lambda_4)\left[\frac{\frac{\left(G_{a,eq}^2e^{\alpha_{w,J}}-G_{w,J}^2e^{\alpha_{a,eq}}\right)\left(e^{\alpha_{w,J}}-e^{\alpha_{a,eq}}\right)}{G_{a,eq}^2G_{w,J}^2\left(e^{\alpha_{w,J}}-e^{\alpha_{a,eq}}\right)^2}-}{\frac{\left(G_{a,eq}e^{\alpha_{w,J}}-G_{w,J}e^{\alpha_{a,eq}}\right)^2}{G_{a,eq}^2G_{w,J}^2\left(e^{\alpha_{w,J}}-e^{\alpha_{a,eq}}\right)^2}}\right],\tag{A.2}$$

where

$$G_{a,eq}=\varphi m_a c_{p,ea},\ G_{w,J}=m_{w,J}c_{p,w},\ \alpha_{a,eq}=\frac{(KA)_2}{\varphi m_a c_{p,a}},\ \alpha_{w,E}=\frac{(KA)_2c_{p,ea}}{m_{w,J}c_{p,w}c_{p,a}}.$$

The differential of Eq. (22) with respect to the thermal conductance $(KA)_3$ yields

$$\frac{\partial F}{\partial (KA)_3}=1-\lambda_4Q_3\left[\frac{\left(G_{w,H}^2e^{\alpha_{a,M}}-G_{a,M}^2e^{\alpha_{w,H}}\right)\left(e^{\alpha_{a,M}}-e^{\alpha_{w,H}}\right)-\left(G_{w,H}e^{\alpha_{a,M}}-G_{a,M}e^{\alpha_{w,H}}\right)^2}{G_{w,H}^2G_{a,M}^2\left(e^{\alpha_{a,M}}-e^{\alpha_{w,H}}\right)^2}\right],\tag{A.3}$$

where

$$G_{a,M}=(1-\varphi)m_a c_{p,a},\ G_{w,H}=m_{w,H}c_{p,w},\ \alpha_{a,M}=\frac{(KA)_3}{(1-\varphi)m_a c_{p,a}},$$

$$\alpha_{w,H}=\frac{(KA)_3}{m_{w,H}c_{p,w}}.$$

The differential of Eq. (22) with respect to the thermal conductance $(KA)_4$ yields

$$\frac{\partial F}{\partial (KA)_4}=1-\lambda_2(Q_c-Q_3)\left[\frac{e^{\alpha_{w,G}}\left(e^{\alpha_{w,G}}-1\right)-e^{2\alpha_{w,G}}}{G_{w,G}^2\left(e^{\alpha_{w,G}}-1\right)^2}\right],\tag{A.4}$$

where

$$G_{w,G}=m_{w,G}c_{p,w},\ \alpha_{w,G}=\frac{(KA)_4}{m_{w,G}c_{p,w}}.$$

The differential of Eq. (22) with respect to the thermal conductance $m_{w,E}$ yields

$$\frac{\partial F}{\partial m_{w,E}}=\lambda_1-\lambda_3Q_1\left[\frac{G_{a,A}c_{p,w}e^{\alpha_{w,E}}\left(e^{\alpha_{a,A}}-e^{\alpha_{w,E}}\right)+\frac{e^{\alpha_{w,E}}}{m_{w,E}}(G_{a,A}-G_{w,E})(KA)_1e^{\alpha_{a,A}}}{G_{a,A}G_{w,E}^2\left(e^{\alpha_{a,A}}-e^{\alpha_{w,E}}\right)^2}\right],\tag{A.5}$$

The differential of Eq. (22) with respect to the thermal conductance $m_{w,G}$ yields

$$\frac{\partial F}{\partial m_{w,G}}=\left[\begin{array}{l}\lambda_1-\lambda_2(Q_c-Q_3)\frac{\frac{(KA)_4}{m_{w,G}}e^{\alpha_{w,G}}-c_{p,w}\left(e^{\alpha_{w,G}}-1\right)}{G_{w,G}^2\left(e^{\alpha_{w,G}}-1\right)^2}+\lambda_4\frac{(Q_c-Q_3)}{m_{w,G}^2c_{p,w}}\\ -\lambda_4Q_3\frac{G_{a,M}c_{p,w}e^{\alpha_{w,G}}\left(e^{\alpha_{a,M}}-e^{\alpha_{w,G}}\right)+\frac{e^{\alpha_{w,G}}}{m_{w,G}}\left(G_{a,M}-G_{w,G}\right)(KA)_3e^{\alpha_{a,M}}}{G_{a,M}G_{w,G}^2\left(e^{\alpha_{a,M}}-e^{\alpha_{w,G}}\right)^2}\end{array}\right],\tag{A.6}$$

The differential of Eq. (22) with respect to the thermal conductance φ yields

$$\frac{\partial F}{\partial \varphi}=-(\lambda_2+\lambda_3+\lambda_4)\left(Q_2\frac{\partial R_2}{\partial \varphi}+\frac{Q_1m_a}{m_{a,A}^2c_{p,ea}}\right)-\lambda_3Q_1\frac{\partial R_1}{\partial \varphi}-\lambda_4Q_3\frac{\partial R_3}{\partial \varphi},\tag{A.7}$$

where

$$\frac{\partial R_1}{\partial \varphi}=\frac{m_ac_{p,a}G_{w,E}e^{\alpha_{a,A}}\left(e^{\alpha_{w,E}}-e^{\alpha_{a,A}}\right)+\frac{1}{\varphi}e^{\alpha_{w,E}}e^{\alpha_{a,A}}(KA)_1(G_{w,E}-G_{a,A})}{G_{a,A}^2G_{w,E}\left(e^{\alpha_{a,A}}-e^{\alpha_{w,E}}\right)^2},$$

$$\frac{\partial R_2}{\partial \varphi}=\frac{m_ac_{p,ea}G_{w,J}e^{\alpha_{ea}}\left(e^{\alpha_{w,J}}-e^{\alpha_{ea}}\right)+\frac{c_{p,ea}}{c_{p,a}\varphi}e^{\alpha_{w,J}}e^{\alpha_{ea}}(KA)_2\left(G_{w,J}-G_{ea}\right)}{G_{ea}^2G_{w,J}\left(e^{\alpha_{w,J}}-e^{\alpha_{ea}}\right)^2},$$

$$\frac{\partial R_3}{\partial \varphi}=\frac{m_ac_{p,a}G_{w,G}e^{\alpha_{a,M}}\left(e^{\alpha_{a,M}}-e^{\alpha_{w,G}}\right)+\frac{1}{1-\varphi}e^{\alpha_{w,G}}e^{\alpha_{a,M}}(KA)_3(G_{a,M}-G_{w,G})}{G_{a,M}^2G_{w,G}\left(e^{\alpha_{a,M}}-e^{\alpha_{w,G}}\right)^2}.$$

The differential of Eq. (22) with respect to the thermal conductance Q_1 yields

$$\frac{\partial F}{\partial Q_1}=(\lambda_2+\lambda_3+\lambda_4)\left(\frac{1}{G_{w,J}}+\frac{1}{m_{a,A}c_{p,ea}}-R_2\right)-\lambda_3R_1,\tag{A.8}$$

where

$$R_1=\frac{G_{w,E}e^{\alpha_{a,A}}-G_{a,A}e^{\alpha_{w,E}}}{G_{w,E}G_{a,A}\left(e^{\alpha_{a,A}}-e^{\alpha_{w,E}}\right)}.$$

The differential of Eq. (22) with respect to the thermal conductance Q_3 yields

$$\frac{\partial F}{\partial Q_3}=\lambda_2R_4+\lambda_4\left(\frac{1}{G_{w,H}}-R_3\right),\tag{A.9}$$

where

$$R_3=\frac{G_{w,G}e^{\alpha_{a,M}}-G_{a,M}e^{\alpha_{w,G}}}{G_{w,G}G_{a,M}\left(e^{\alpha_{a,M}}-e^{\alpha_{w,G}}\right)},$$

$$R_4=\frac{e^{\alpha_{w,G}}}{G_{w,G}\left(e^{\alpha_{w,G}}-1\right)}.$$

References

[1] A. Costa, M.M. Keane, J.I. Torrens, E. Corry, Building operation and energy performance: monitoring, analysis and optimisation toolkit, Appl. Energy 101 (2013) 310–316, https://doi.org/10.1016/j.apenergy.2011.10.037.

[2] B. Porumb, P. Ungureşan, L.F. Tutunaru, A. Şerban, M. Bălan, A review of indirect evaporative cooling technology, Energy Procedia 85 (2016) 461–471, https://doi.org/10.1016/j.egypro.2015.12.228.

[3] X. Cui, K.J. Chua, W.M. Yang, Numerical simulation of a novel energy-efficient dew-point evaporative air cooler, Appl. Energy 136 (2014) 979–988, https://doi.org/10.1016/j.apenergy.2014.04.040.

[4] M. Lemouari, M. Boumaza, A. Kaabi, Experimental analysis of heat and mass transfer phenomena in a direct contact evaporative cooling tower, Energy Convers. Manage. 50 (2009) 1610–1617, https://doi.org/10.1016/j.enconman.2009.02.002.

[5] C. Zhan, Z. Duan, X. Zhao, S. Smith, H. Jin, S. Riffat, Comparative study of the performance of the M-cycle counter-flow and cross-flow heat exchangers for indirect evaporative cooling – Paving the path toward sustainable cooling of buildings, Energy 36 (2011) 6790–6805, https://doi.org/10.1016/j.energy.2011.10.019.

[6] M. Lemouari, M. Boumaza, Experimental investigation of the performance characteristics of a counterflow wet cooling tower, Int. J. Therm. Sci. 49 (2010) 2049–2056, https://doi.org/10.1016/j.ijthermalsci.2010.05.012.

[7] X. Cui, K.J. Chua, W.M. Yang, K.C. Ng, K. Thu, V.T. Nguyen, Studying the performance of an improved dew-point evaporative design for cooling application, Appl. Therm. Eng. 63 (2014) 624–633, https://doi.org/10.1016/j.applthermaleng.2013.11.070.

[8] G. Heidarinejad, M. Bozorgmehr, S. Delfani, J. Esmaeelian, Experimental investigation of two-stage indirect/direct evaporative cooling system in various climatic conditions, Build. Environ. 44 (2009) 2073–2079, https://doi.org/10.1016/j.buildenv.2009.02.017.

[9] B. Tashtoush, M. Tahat, A. Al-Hayajneh, V.A. Mazur, D. Probert, Thermodynamic behaviour of an air-conditioning system employing combined evaporative-water and air coolers, Appl. Energy 70 (2001) 305–319, https://doi.org/10.1016/S0306-2619(01)00039-3.

[10] P. Mazzei, A. Palombo, Economic evaluation of hybrid evaporative technology implementation in Italy, Build. Environ. 34 (1999) 571–582, https://doi.org/10.1016/S0360-1323(98)00049-3.

[11] F. Al-Sulaiman, Evaluation of the performance of local fibers in evaporative cooling, Energy Convers. Manage. 43 (2002) 2267–2273, https://doi.org/10.1016/S0196-8904(01)00121-2.

[12] X. Zhao, J.M. Li, S.B. Riffat, Numerical study of a novel counter-flow heat and mass exchanger for dew point evaporative cooling, Appl. Therm. Eng. 28 (2008) 1942–1951, https://doi.org/10.1016/j.applthermaleng.2007.12.006.

[13] M. Farmahini-Farahani, S. Delfani, J. Esmaeelian, Exergy analysis of evaporative cooling to select the optimum system in diverse climates, Energy 40 (2012) 250–257, https://doi.org/10.1016/j.energy.2012.01.075.

[14] F. Yuan, Q. Chen, Optimization criteria for the performance of heat and mass transfer in indirect evaporative cooling systems, Chin. Sci. Bull. 57 (2012) 687–693, https://doi.org/10.1007/s11434-011-4903-3.
[15] T. Muangnoi, W. Asvapoositkul, S. Wongwises, Effects of inlet relative humidity and inlet temperature on the performance of counterflow wet cooling tower based on exergy analysis, Energy Convers. Manage. 49 (2008) 2795–2800, https://doi.org/10.1016/j.enconman.2008.03.019.
[16] Y. Jiang, X. Xie, Theoretical and testing performance of an innovative indirect evaporative chiller, Sol. Energy 84 (2010) 2041–2055, https://doi.org/10.1016/j.solener.2010.09.012.
[17] A. Khaliq, I. Dincer, Energetic and exergetic performance analyses of a combined heat and power plant with absorption inlet cooling and evaporative aftercooling, Energy 36 (2011) 2662–2670, https://doi.org/10.1016/j.energy.2011.02.007.
[18] A. Afram, F. Janabi-Sharifi, Review of modeling methods for HVAC systems, Appl. Therm. Eng. 67 (2014) 507–519, https://doi.org/10.1016/j.applthermaleng.2014.03.055.
[19] T.R. Kiran, S.P.S. Rajput, An effectiveness model for an indirect evaporative cooling (IEC) system: comparison of artificial neural networks (ANN), adaptive neuro-fuzzy inference system (ANFIS) and fuzzy inference system (FIS) approach, Appl. Soft Comput. 11 (2011) 3525–3533, https://doi.org/10.1016/j.asoc.2011.01.025.
[20] A. Sohani, H. Sayyaadi, S. Hoseinpoori, Modeling and multi-objective optimization of an M-cycle cross-flow indirect evaporative cooler using the GMDH type neural network, Int. J. Refrig 69 (2016) 186–204, https://doi.org/10.1016/j.ijrefrig.2016.05.011.
[21] B. Halasz, A general mathematical model of evaporative cooling devices, Revue Générale de Thermique 37 (1998) 245–255, https://doi.org/10.1016/S0035-3159(98)80092-5.
[22] J.-U.-R. Khan, M. Yaqub, S.M. Zubair, Performance characteristics of counter flow wet cooling towers, Energy Convers. Manage. 44 (2003) 2073–2091, https://doi.org/10.1016/S0196-8904(02)00231-5.
[23] A. Pakari, S. Ghani, Comparison of 1D and 3D heat and mass transfer models of a counter flow dew point evaporative cooling system: Numerical and experimental study, Int. J. Refrig. 99 (2019) 114–125, https://doi.org/10.1016/j.ijrefrig.2019.01.013.
[24] Q. Chen, J.-H. Hao, T. Zhao, An alternative energy flow model for analysis and optimization of heat transfer systems, Int. J. Heat Mass Transf. 108 (2017) 712–720, https://doi.org/10.1016/j.ijheatmasstransfer.2016.12.080.
[25] Q. Chen, R.-H. Fu, Y.-C. Xu, Electrical circuit analogy for heat transfer analysis and optimization in heat exchanger networks, Appl. Energy 139 (2015) 81–92, https://doi.org/10.1016/j.apenergy.2014.11.021.
[26] T. Zhao, Y. Min, Q. Chen, J.-H. Hao, Electrical circuit analogy for analysis and optimization of absorption energy storage systems, Energy 104 (2016) 171–183, https://doi.org/10.1016/j.energy.2016.03.120.
[27] K. Hu, L. Chen, Q. Chen, X.-H. Wang, J. Qi, F. Xu, Y. Min, Phase-change heat storage installation in combined heat and power plants for integration of renewable energy sources into power system, Energy 124 (2017) 640–651, https://doi.org/10.1016/j.energy.2017.02.048.
[28] G. Shen, F. Yuan, Y. Li, W. Liu, The energy flow method for modeling and optimization of Organic Rankine Cycle (ORC) systems, Energy Convers. Manage. 199 (2019) 111958, https://doi.org/10.1016/j.enconman.2019.111958.
[29] F. Yuan, Q. Chen, A property diagram-based method for synthesis and parameter optimization of heat and mass transfer in moist air–water/aqueous solution systems, Int. J. Heat Mass Transf. 87 (2015) 189–200, https://doi.org/10.1016/j.ijheatmasstransfer.2015.03.082.
[30] F. Yuan, Q. Chen, A global optimization method for evaporative cooling systems based on the entransy theory, Energy 42 (2012) 181–191, https://doi.org/10.1016/j.energy.2012.03.070.
[31] Y.-C. Xu, Q. Chen, Z.-Y. Guo, Optimization of heat exchanger networks based on Lagrange multiplier method with the entransy balance equation as constraint, Int. J. Heat Mass Transf. 95 (2016) 109–115, https://doi.org/10.1016/j.ijheatmasstransfer.2015.11.092.
[32] S.-Y. Zhao, Q. Chen, Design criteria of different heat exchangers for the optimal thermodynamic performance of regenerative refrigeration systems, Appl. Therm. Eng. 93 (2016) 1164–1174, https://doi.org/10.1016/j.applthermaleng.2015.10.031.
[33] J.-H. Hao, Q. Chen, J.-X. Ren, M.-Q. Zhang, J. Ai, An experimental study on the offset-strip fin geometry optimization of a plate-fin heat exchanger based on the heat current model, Appl. Therm. Eng. 154 (2019) 111–119, https://doi.org/10.1016/j.applthermaleng.2019.03.072.
[34] Q. Chen, N. Pan, Z.-Y. Guo, A new approach to analysis and optimization of evaporative cooling system II: Applications, Energy 36 (2011) 2890–2898, https://doi.org/10.1016/j.energy.2011.02.031.